N O T I C E

THIS DOCUMENT HAS BEEN REPRODUCED FROM MICROFICHE. ALTHOUGH IT IS RECOGNIZED THAT CERTAIN PORTIONS ARE ILLEGIBLE, IT IS BEING RELEASED IN THE INTEREST OF MAKING AVAILABLE AS MUCH INFORMATION AS POSSIBLE

NASA Technical Memorandum 81672

Numerical Simulation of Flows in Curved Diffusers with Cross-Sectional Transitioning Using a Three-Dimensional Viscous Analysis

C. E. Towne and B. H. Anderson
Lewis Research Center
Cleveland, Ohio

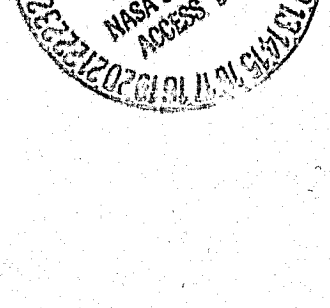

Prepared for the
Nineteenth Aerospace Sciences Meeting
sponsored by the American Institute of Aeronautics and Astronautics
St. Louis, Missouri, January 12-15, 1981

NASA

NUMERICAL SIMULATION OF FLOWS IN CURVED DIFFUSERS WITH CROSS-SECTIONAL TRANSITIONING USING A THREE-DIMENSIONAL VISCOUS ANALYSIS

by C. E. Towne* and B. H. Anderson**

National Aeronautics and Space Administration
Lewis Research Center
Cleveland, Ohio 44135

SYMBOLS

$p_{1\text{-}D}$	one-dimensional pressure correction
$p_{3\text{-}D}$	three-dimensional inviscid pressure field
u_1, u_2, u_3	local Cartesian velocities
x_1, x_2, x_3	local Cartesian coordinates
y_1, y_2, y_3	curvilinear computational coordinates
δ	Kronecker delta
μ_ℓ	effective viscosity
ρ	density
ϕ	velocity potential for irrotational component of secondary flow
ψ	stream function for rotational component of secondary flow
Ω	streamwise vorticity

INTRODUCTION

Three-dimensional subsonic diffusers are relatively common in modern air-breathing propulsion systems. The shape of the duct cross-section may vary in the streamwise direction, and offset bends are often present. Strong

---

*Aerospace Engineer; Member, AIAA.
**Head Aerodynamics Analysis Section; Member, AIAA.

secondary flows can thus be generated. In addition, since the flow is diffusing, the boundary layer may grow until its thickness is comparable to the duct radius. These phenomena have important effects on overall diffuser performance and engine/inlet compatibility.

Conventional boundary layer methods cannot properly analyze these complex flows. A complete three-dimensional Navier-Stokes analysis could be used, but extremely large amounts of computer time and storage would be required for a detailed solution, thus precluding the use of such an analysis for routine calculation using present computer technology.

However, if it is assumed that a primary flow direction can be identified, certain approximations can be made in the Navier-Stokes equations, resulting in a set of equations for fully viscous, subsonic, compressible flow that can be solved by forward marching. One such method, designated PEPSIG, was developed by Briley and McDonald[1], and recently modified by Levy, McDonald, Briley, and Kreskovsky[2]. This paper presents the results of the first in a series of studies to evaluate the PEPSIG analysis.

GOVERNING EQUATIONS

In this analysis, the flow is computed by a spatial marching procedure which solves an approximate form of the Navier-Stokes equations. Three basic assumptions are made. First, it is assumed that the flow is primarily in the direction of the duct centerline, with transverse secondary flow. Second, the pressure field is represented by the sum of a previously determined three-dimensional pressure field and a one-dimensional pressure correction computed as part of the marching analysis. And finally, second derivatives in the primary flow direction are assumed negligible.

The derivation of the governing equations actually solved in the PEPSIG analysis is fairly complex, and has been presented elsewhere[2]. For completeness, however, a brief discussion is presented here. The equations are first written in local Cartesian coordinates x_1, x_2, and x_3, with corresponding velocities u_1, u_2, and u_3. The x_3 direction is the primary flow direction, and is aligned with the duct centerline at each marching step. The x_1 and x_2 directions define the transverse, or secondary flow plane. The equations are then transformed into general non-orthogonal, body-fitted, curvilinear coordinates y_1, y_2, and y_3.

The x_3 momentum equation is then given, using tensor notation, by:

$$\rho u_j \frac{\partial y_i}{\partial x_j}\frac{\partial u_3}{\partial y_i} = -\frac{\partial y_i}{\partial x_3}\frac{\partial p_{3-D}}{\partial y_i} - \frac{\partial y_3}{\partial x_3}\frac{\partial p_{1-D}}{\partial y_3} + \frac{\partial y_i}{\partial x_j}\frac{\partial}{\partial y_i}\left\{\mu_\ell\left[(\bar{1} - \delta_{j3})\left(\frac{\partial y_n}{\partial x_j}\frac{\partial u_3}{\partial y_n} + \frac{\partial y_n}{\partial x_3}\frac{\partial u_j}{\partial y_n}\right) - \frac{2}{3}\delta_{3j}(1 - \delta_{k3})\frac{\partial y_n}{\partial x_k}\frac{\partial u_k}{\partial y_n}\right]\right\} \qquad (1)$$

Here $p_{3-D} = p_{3-D}\,(x_1, x_2, x_3)$ is the known three-dimensional pressure field and $p_{1-D} = p_{1-D}\,(x_3)$ is the correction computed during the marching solution. In the present study, p_{3-D} was computed using a three-dimensional potential flow analysis .

The differential continuity equation is written in terms of a scalar potential ϕ as:

$$\frac{\partial y_j}{\partial x_i}\frac{\partial}{\partial y_j}\left(\rho\frac{\partial y_k}{\partial x_i}\right)\frac{\partial \phi}{\partial y_k} + \rho\left(\frac{\partial y_k}{\partial x_i}\right)^2\frac{\partial^2 \phi}{\partial y_k^2} + 2\rho\frac{\partial y_1}{\partial x_i}\frac{\partial y_2}{\partial x_i}\frac{\partial^2 \phi}{\partial y_1 \partial y_2} = -\frac{\partial y_n}{\partial x_3}\frac{\partial \rho u_3}{\partial y_n} \qquad (2)$$

The x_1 and x_2 momentum equations are combined to form an equation for vorticity transport in the x_3 direction and a cross-plane stream function equation. After some simplifications, the vorticity equation is given by:

$$u_j \frac{\partial \Omega_3}{\partial x_j} - \Omega_j \frac{\partial u_3}{\partial x_j} = \frac{\mu_\ell}{\rho} \frac{\partial^2 \Omega_3}{\partial x_j^2} \tag{3}$$

and the stream function equation by:

$$\frac{\partial y_j}{\partial x_i} \frac{\partial}{\partial y_j} \left(\frac{1}{\rho} \frac{\partial y_k}{\partial x_i} \right) \frac{\partial \psi}{\partial y_k} + \frac{1}{\rho} \left(\frac{\partial y_k}{\partial x_i} \right)^2 \frac{\partial^2 \psi}{\partial y_k^2}$$

$$+ \frac{2}{\rho} \frac{\partial y_1}{\partial x_i} \frac{\partial y_2}{\partial x_i} \frac{\partial^2 \psi}{\partial y_1 \partial y_2} = -\Omega_3 \tag{4}$$

The energy equation is eliminated by assuming constant total enthalpy. A mixing length turbulence model is used, with the distribution of mixing length given by the Buleev formula[3]. The boundary conditions used result in no-slip at the walls, and symmetry at the symmetry plane.

The above equations are solved by forward marching from an initial station, where the flow profiles are known, using an implicit numerical technique. Details of the solution procedure are given in references 1 and 2.

COMPUTED RESULTS

Circular S-Duct

As an initial test of the ability of the PEPSIG analysis to correctly predict the basic physical phenomena present in curved ducts, a simple circular S-duct was run. The duct had a diameter of .61 m. (2 ft.) and the centerline was offset one diameter in a streamwise distance of five diameters. The flow was laminar, with an entrance Mach

number of .2 and a Reynolds number based on diameter of 2000. The initial boundary layer thickness was 3.0 cm. (.1 ft.). This case was run with a 20x20 mesh in the cross-plane, and 41 streamwise stations. The calculation required 16 minutes on an IBM 370/3033.

Computed total pressure contours are shown at several stations along the duct in figure 1. The boundary layer growth along the top of the duct in the first bend can be clearly seen. In the second half of the duct, this region of low energy flow expands greatly, forming a pocket of low total pressure at the top of the duct. This phenomenon has been seen in several experiments[4-5]. A comparison between the analytical results and the results from one of these experiments[4] is presented in figure 2. Here total pressure contours at the exit plane are plotted for both cases. Although only a qualitative comparison can be made since the tested case was for a different geometry and flow conditions than the computed case, the basic physics of the flow appear to have been computed correctly.

The mechanism by which the pocket of low energy flow is formed has been presented by Bansod and Bradshaw[4]. This mechanism is present in the analytical results, and can be explained by examining the cross-flow velocity vectors, as shown in figure 3. Except for the results at station 5, which is 1/4 of the way through the first bend, the vector plots are shown at the same stations as the total pressure plots in figure 1. In the first half of the duct (stations 1-21), the classic secondary flow pattern for flow through a curved pipe is set up. The low speed boundary layer fluid migrates circumferentially from the pressure surface toward the suction surface, and the essentially inviscid core flow responds to centrifugal forces. A pair of contra-rotating vortices is thus established. In the second bend (stations 21-41), these vortices are intensified, and become centered

near the top of the duct. As the low energy fluid approaches the symmetry plane from both sides, it erupts from the surface forming the pocket of low total pressure characteristic of S-duct flows.

F-16 Inlet

To evaluate the ability of the analysis to compute the flow through a realistic diffuser configuration, calculations were made for subsonic flow in the F-16 inlet[6]. A schematic diagram of this inlet is given in figure 4. Cross-sections are shown at various stations along the inlet. The station numbers are fuselage stations from reference 6. The inlet has a generally S-shaped centerline, with the first and second bends separated by a straight section. The total offset is .616 m. (2.02 ft.) and the length from the throat to the engine face is 4.74 m. (15.55 ft.). The cross-section shape transitions from slightly smile-shaped at the throat to circular at the engine face. The overall area ratio is 1.33.

The non-orthogonal, body fitted mesh generator currently used in the PEPSIG analysis requires super-elliptic cross-section shapes[7]. Meshes can thus be generated for ducts with cross-sections that vary from nearly rectangular or square (with a large super-ellipse exponent) to elliptical or circular (with an exponent of 2). The actual F-16 cross-sections could therefore not be modeled exactly. Instead, the following procedure was used. At each streamwise station, the major axis of the super-ellipse was chosen to match the maximum spanwise dimension of the actual cross-section. The minor axis used was the gapwise distance in the symmetry plane of the inlet. The super-ellipse exponent was then computed to give the correct area, but was not allowed to fall below 2, corresponding to an ellipse. The result was the baseline configuration shown in figure 5a.

A calculation was made for turbulent flow in this configuration at a Reynolds number per meter of 1.44×10^7 (4.4×10^6 per foot) and a free stream Mach number of .9. The initial boundary layer thickness specified was .91 cm, (.36 in.). These flow conditions correspond to one of the test conditions of reference 6. A 24x24 mesh was used in the cross-plane, with 250 streamwise stations. The calculation required about 2 1/2 hours on an IBM 370/3033.

Computed total pressure contours are shown at several stations along the duct in figure 6. Boundary layer growth around the entire circumference is evident through the first half of the duct. About halfway through the duct, the boundary layers at the top and bottom start growing more rapidly, while near the sides the boundary layer becomes thinner.

The surprising aspect of this calculation was the degree of symmetry between the contours in the top and bottom halves of the duct. Based on the S-duct calculations presented earlier, as well as experimental results for S-ducts, it had been expected that secondary flow vortices would be generated by the centerline curvature and would cause a shift in the total pressure contours. A comparison of computed and experimental exit plane total pressure contours is presented in figure 7. The data are from reference 8, and are for a somewhat different geometry and incoming flow than was used in the analysis. (In the test, the inlet had an external ramp forebody and a compressor face hub, and was run at a 1 degree angle of attack. The Reynolds number was 4.9×10^6 per meter (1.5×10^6 per foot) and the free stream Mach number was .8). The experimental results, however, are similar to the computed results in the degree of symmetry between the upper and lower halves of the inlet. It should be noted that the computed boundary layer grows very quickly during the first few marching steps.

This is believed to be caused by appreciable numerical diffusion in this thin boundary layer calculation as a result of inadequate mesh resolution. This resulted in larger calculated total pressure losses than were measured experimentally. With proper mesh resolution, this problem should be alleviated.

It was then hypothesized that the effect of the change in cross-section shape was much more important in this flow than the effect of the centerline curvature. To verify this hypothesis, two additional geometries were run. The first, shown in figure 5b, had the same distribution of cross-section shape as the baseline configuration, but with a straight centerline. The second, shown in figure 5c, had the same centerline shape and area distribution as the baseline configuration, but with circular cross-sections. These configurations were chosen to isolate the effects of shape change and centerline curvature. The flow conditions and grid were the same as for the baseline calculation.

The total pressure contours for the straight centerline configuration are shown in figure 8, and are virtually identical to those for the baseline configuration. The results for the circular cross-section case, shown in figure 9, do show a slight shift in the total pressure contours, indicating that the centerline curvature is strong enough to generate at least a weak secondary flow vortex. This is confirmed when the cross-flow velocities are examined. The computed secondary flow velocity vectors at the exit plane for all three F-16 configurations are shown in figure 10. The secondary flow patterns for the baseline and straight centerline configurations are basically similar. Although some influence of centerline curvature can be seen in the baseline results, no vortex pattern is set up. The circular cross-section configuration, however, has an obvious secondary flow vortex at the exit plane.

Additional insight can be gained by examining the circumferential pressure gradient in the baseline F-16 configuration. In figure 11a the inviscid static pressure is plotted for a cross-section at about the mid-point of the duct. The pressure is higher in the region of the converging sides of the cross-section than at the diverging top and bottom. The low energy boundary layer fluid is thus driven in both directions away from the sides of the inlet, causing the boundary layer thickness to decrease there and to increase at the top and bottom of the inlet. By the time the second bend is reached, most of the cross-section transitioning has been completed. The circumferential pressure distribution in the second bend, shown in figure 11b, is similar to that found in the second bend of a constant area S-duct. However, the boundary layer has become so thin near the converging sides of the duct that the boundary layers in the top and bottom halves of the inlet are essentially isolated from each other. Low energy boundary layer fluid cannot migrate through this thin boundary layer region, and therefore no secondary flow vortex is formed. In the circular cross-section configuration, of course, the boundary layer does not thin out at the sides of the duct, and a vortex pattern is generated. Thus, although the centerline curvature in the baseline F-16 configuration is strong enough to produce a secondary flow vortex, the changing cross-section shape suppresses its formation.

CONCLUDING REMARKS

1. The PEPSIG analysis gives at least qualitatively correct predictions of the development of secondary flow vortices and total pressure distortion in S-shaped ducts.

2. More detailed quantitative comparisons with experiment are needed to determine the accuracy of the analysis.

3. Mesh studies are needed to determine the resolution required for thin boundary layer calculations.

4. The analysis can be used to help understand the development of secondary flow phenomena in complex configurations.

5. There is a critical need for detailed experimental data on secondary flow development in ducts with centerline curvature and/or cross-section transitioning for proper code evaluation.

REFERENCES

1. Briley, W. R. and McDonald, H., "Analysis and Computation of Viscous Subsonic Primary and Secondary Flows," AIAA Paper 79-1453, July 1979.

2. Levy, R., McDonald, H., Briley, W. R., and Kreskovsky, J. P., "A Three-Dimensional Turbulent Compressible Subsonic Duct Flow Analysis for Use with Constructed Coordinate Systems," AIAA Paper 80-1398, July 1980.

3. Buleev, N. I., "Theoretical Model of the Mechanisms of Turbulent Exchange in Fluid Flow," Atomic Energy Research Establishment, U. K., AERE-Trans-957, 1963.

4. Bansod, P. and Bradshaw, R., "The Flow in S-Shaped Ducts," Aeronautical Quarterly, Vol. 23, Pt. 2, May 1972, pp. 131-140.

5. Rowe, M., "Measurements and Computations of Flow in Pipe Bends," Journal of Fluid Mechanics, Vol. 43, Pt. 4, pp. 771-783.

6. Leamer, P. C. and Kennon, I. G., "Experimental Investigation of a 0.15 Scale Model of an Underfuselage Normal-Shock Inlet," NASA CR-3049, 1978.

7. Eiseman, P. R., McDonald, H., and Briley, W. R., "A Method for Computing Three-Dimensional Viscous Diffuser Flows," United Technologies Research Center, East Hartford, CT, R75-911737-1, July 1975.

8. Hawkins, J. E., "Experimental Investigation of a 0.15-Scale Model of a Conformal Variable-Ramp Inlet for the F-16 Airplane," General Dynamics, Fort Worth, TX, ERR-FW-2014, Mar. 1980. (NASA CR-159640)

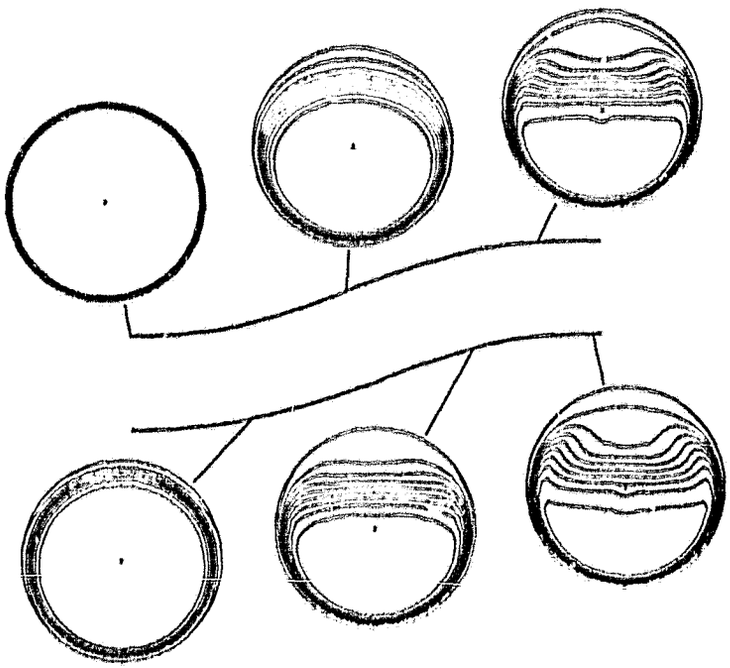

Figure 1. - Computed total pressure contours for circular S-duct.

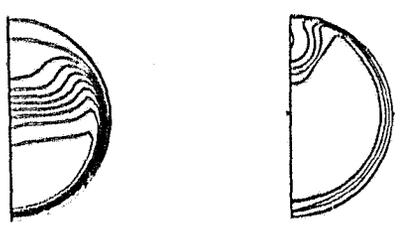

ANALYSIS EXPERIMENT (REF. 4)

Figure 2. - Qualitative comparison between computed and experimental total pressure contours at exit of circular S-duct.

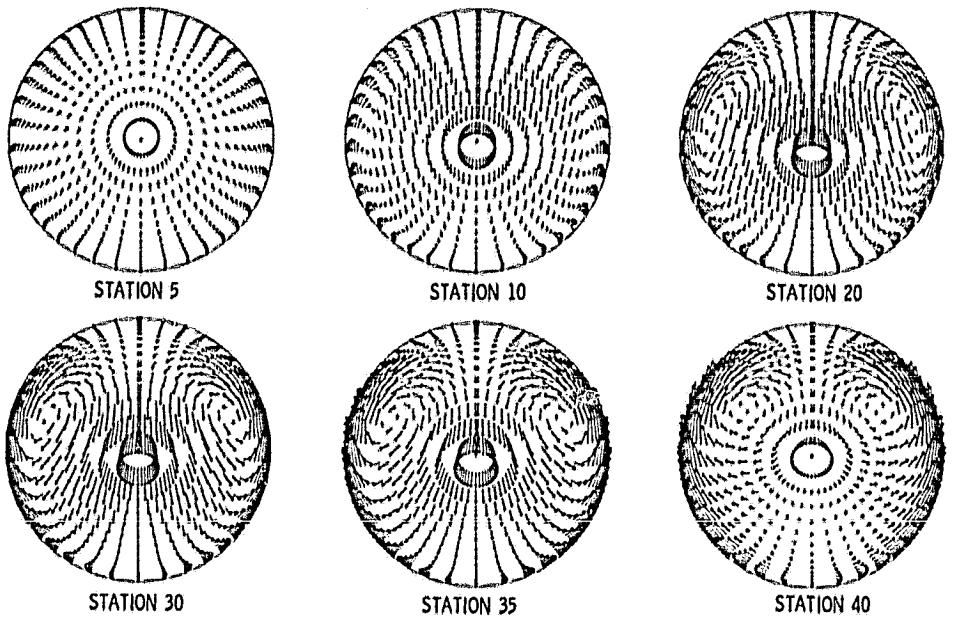

Figure 3. - Computed secondary flow development for circular S-duct.

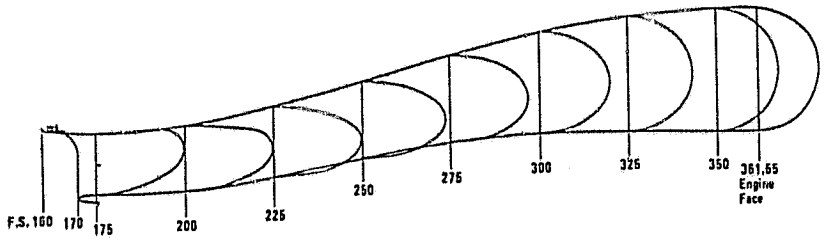

Figure 4. - F-16 inlet geometry.

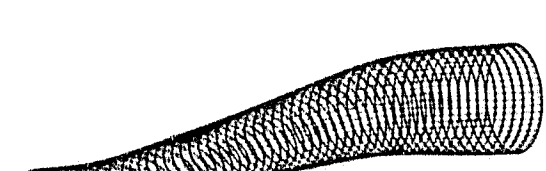

(a) Baseline configuration.

(b) Straight centerline configuration.

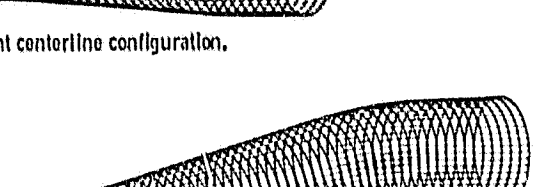

(c) Circular cross-section configuration.

Figure 5. - F-16 inlet geometry breakdown.

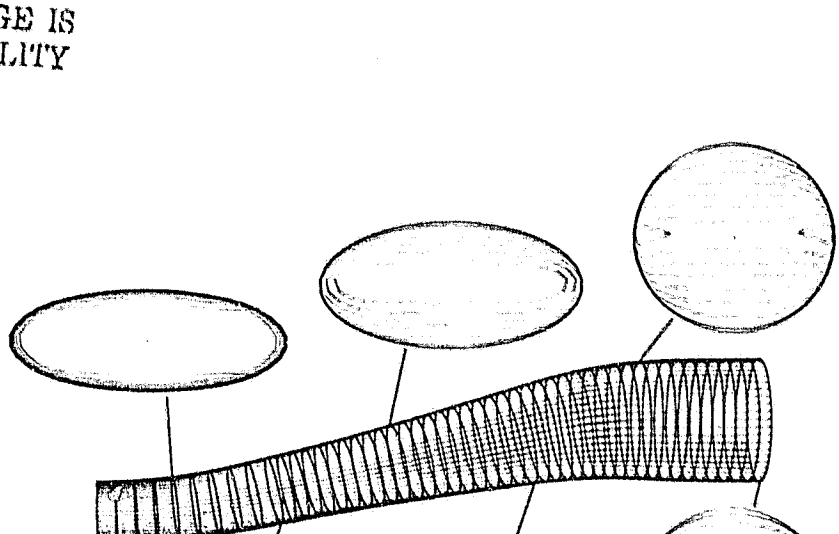

Figure 6. - Computed total pressure contours for F-16 inlet, baseline configuration.

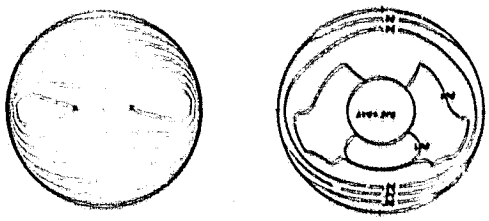

Figure 7. - Qualitative comparison between computed and experimental total pressure contours at exit of F-16 inlet.

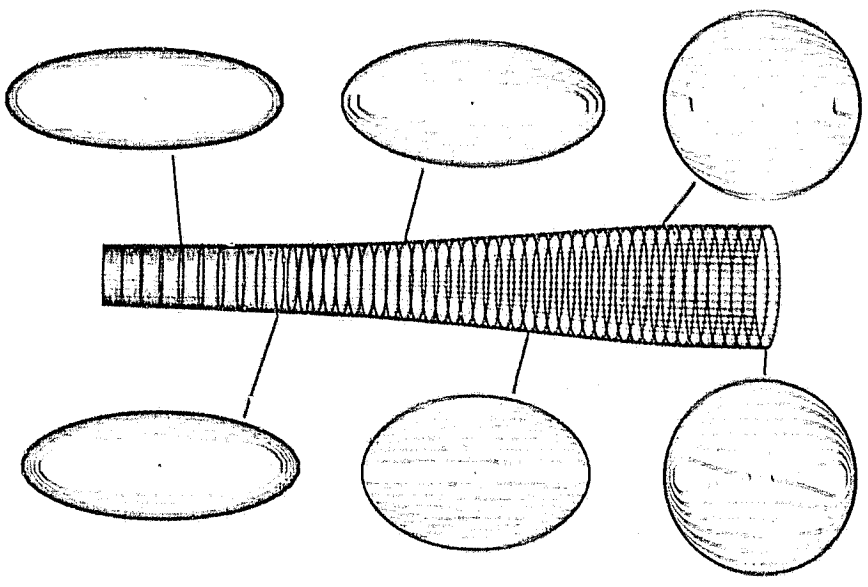

Figure 8. - Computed total pressure contours for F-16 inlet, straight centerline configuration.

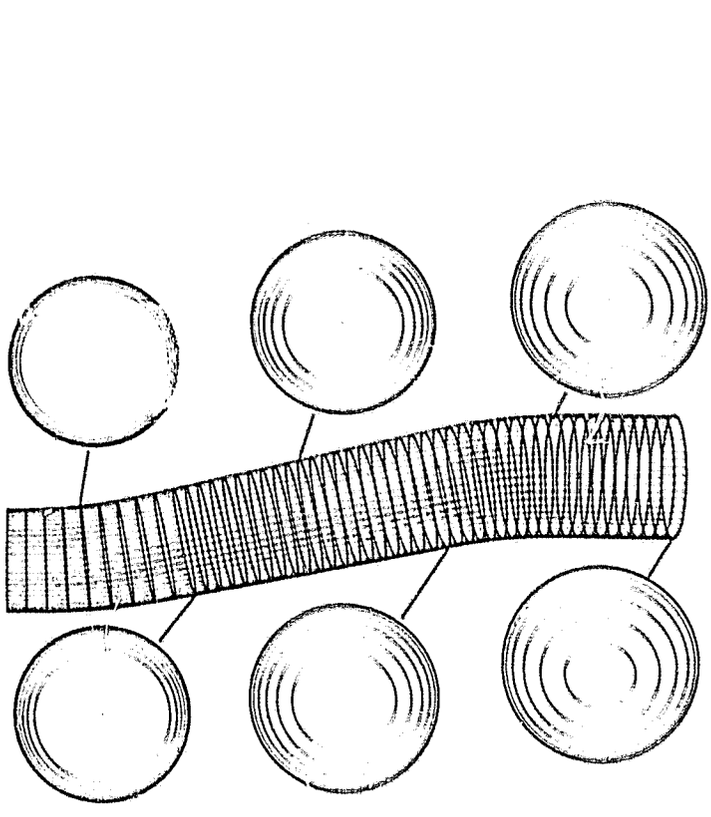

Figure 9. - Computed total pressure contours for F-16 inlet, circular cross-section configuration.

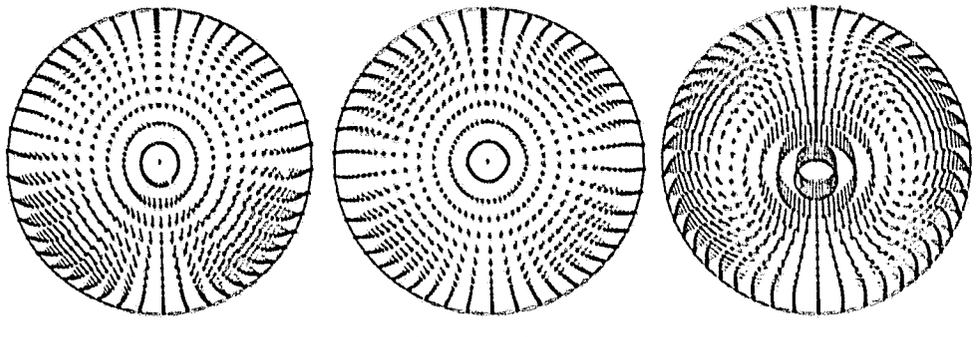

Figure 10. - Computed secondary flow at exit plane of F-16 inlet configurations.

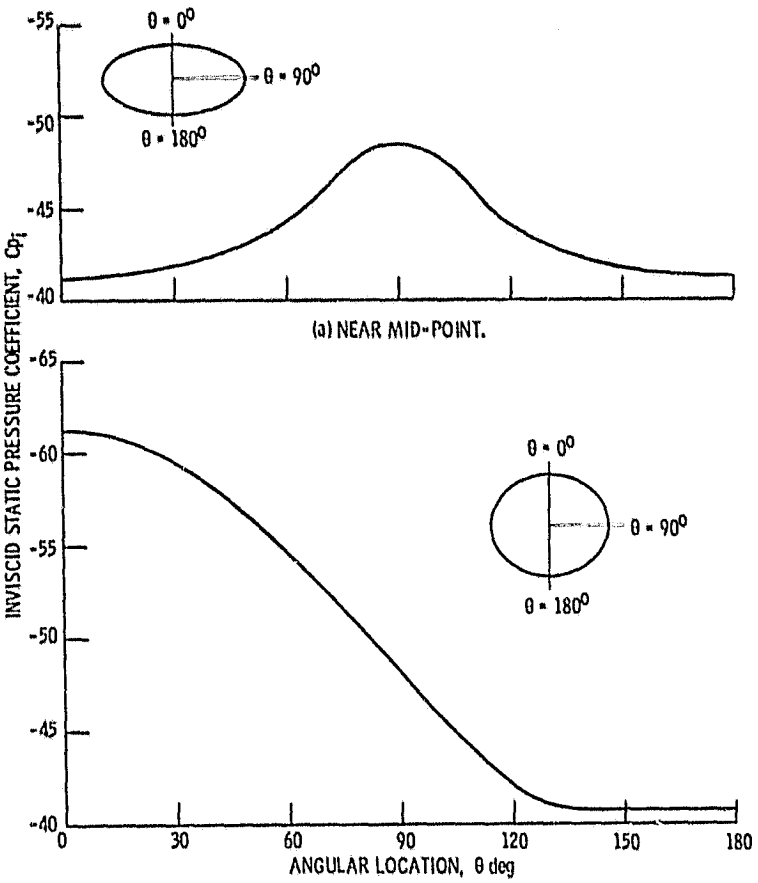

Figure 11. - Circumferential inviscid static pressure distribution of baseline F-16 inlet configuration.